On the Possibility of Intensity Based Registration for Metric Resolution SAR and Optical Imagery

Sahil Suri* and Peter Reinartz
Remote Sensing Technology Institute (IMF) German Aerospace Center (DLR) PO Box 1116, 82230 Wessling, Germany
*Phone: +49 (0)8153 28-2716 *Fax: +49 (0)8153 28-1444
Email: Sahil.Suri@dlr.de, Peter.Reinartz@dlr.de.

Keywords: mutual information, cluster reward algorithm, segmentation, urban areas, image registration

ABSTRACT

Multimodal image registration is a key to many remote sensing tasks like fusion, change detection, GIS overlay operations, 3D visualization etc. With advancements in research, intensity based similarity metrics namely mutual information (MI) and cluster reward algorithm (CRA) have been utilized for intricate multimodal registration problem. The computation of these metrics involves estimating the joint histogram directly from image intensity values, which might have been generated from different sensor geometries and/or modalities (e.g. SAR and optical). Modern day satellites like TerraSAR-X and IKONOS provide high resolution images generating enormous data volume along with very different image radiometric properties (especially in urban areas) not observed ever before. Thus, performance evaluation of intensity based registration techniques for metric resolution imagery becomes an interesting case study. In this paper, we analyze the performance of similarity metrics namely, mutual information and cluster reward algorithm for metric resolution images acquired over both plain and urban/semi-urban areas. Techniques for handling the generated enormous data volume and influence of really different sensor geometries over images especially acquired over urban areas have also been proposed and rightfully analyzed. Our findings from three carefully selected datasets indicate that the intensity based techniques can still be utilized for high resolution imagery but certain adaptations (like compression and segmentation) become useful for meaningful registration results.

1. INTRODUCTION

Last decade has seen an enormous increase in earth observation data in terms of quality, quantity and availability. Recently, there has been a significant increase in the number of high resolution satellites like GeoEye-1, WorldView-1, IKONOS, QUICKBIRD, TerraSAR-X, Cosmo-Skymed and Pleiades. Availability of high resolution images from these satellites with different modalities will further increase the utilization of remote sensing images for practical on ground applications. Already remote sensing images have been utilized for change detection (Li et al., 2006), traffic monitoring (Reinartz et al., 2006), urban damage detection and mapping (Stramondo et al., 2007). Normally, applications need to accommodate images from different sensors/modalities; reason might be specific application demands or data unavailability. For example in case of a natural calamity, decision makers might be forced to use an old archived optical data with a newly acquired (post disaster) SAR image. Combined application of data from different sensors requires georeferenced and fine co-registered images for an accurate and successful analysis. Although, latest satellites provide the end user already georeferenced and orthorectified data products but still registration differences exist between various data sets acquired from different providers. These differences need to be taken care

off through quick automated techniques before using the images in different applications like cartographic mapping, change detection, image fusion, 3D visualization and GIS overlays.

Image registration refers to the task of aligning two or more images acquired at different times, from different sensors or from different view points. Image registration can roughly be classified into categories namely, feature based and intensity based techniques. An extensive overview and survey of various image registration methods used in the above mentioned fields can be found in Brown (1992) and Zitová and Flusser (2003). Specifically, review of registration methods and techniques for remotes sensing imagery are also available (Fonseca and Manjunath, 1996; Wong and Clausi, 2007).

For registration of SAR and optical imagery, intensity based techniques have an advantage over the feature based techniques as successful detection and matching of images from these very different sensors is a meticulous task. For intensity based techniques, the problem of registration is generally mapped as an optimization problem. Where the spatial transformation function *T* is the argument of the optimum of some similarity metric S, applied to reference image IB_{RB} and transformed input image IB_{TIB}. This can be expressed as:

$$T = \arg(opt(S(I_R, I_{TI}))) \quad (1)$$

Registration based on Equation 1 has been successfully utilized for different SAR optical image pairs. Similarity metrics namely, mutual information and cluster reward algorithm (Inglada 2002, Inglada and Giros, 2004) have been utilized for registration in the following scenarios

1) Cluster Reward Algorithm
   i. Different date SPOT multispectral (Inglada, 2002)
   ii. SPOT-4 and ERS-2 (Inglada and Giros, 2004)

2) Mutual Information
   i. Different date SPOT multispectral (Inglada, 2002)
   ii. Landsat-IRS, multitemporal Radarsat, IRS Pan-Radarsat (Chen et al., 2003a,b)
   iii. Landsat-7 and Landsat-5 (Cole Rhodes et al., 2003)
   iv. IRS and compatible Radar (Chen and Varshney, 2000)

A vigilant review of all the above mentioned work mainly done for 5-10m spatial resolution imagery indicates the usefulness of both the intensity based metrics but still there performance for datasets from latest high resolution sensors like TerraSAR-X and IKONOS has not been explored to develop registration strategies for different industrial and academic applications. In general, challenges encountered during intensity based registration of high resolution SAR and optical imagery are:

i. *Data Volume:* Both of the mentioned metrics depend upon the joint histogram of the images being registered. So as the spatial resolution increases to 1m the data volume becomes just huge and leads to undesirable large registration turn around times.

ii. *Geometric and Radiometric Differences:* The increase in spatial resolution further widens the existing gap of sensor geometry and radiometry between the two sensors. As both of the mentioned similarity metrics work directly with intensity values the above mentioned differences can greatly influence the overall registration results (especially in urban areas).

In context of the challenges associated with high resolution imagery, our main objectives might be enumerated as:

i. To show the importance and usefulness of image compression for registration of high resolution SAR and optical imagery.
ii. To analyze the possible influence of different sensor geometries for intensity based registration of metric resolution imagery acquired over urban/semi-urban areas and to study the characteristic behavior of the utilized similarity metrics.

iii. To present a critical comparison between the two explored metrics in context of the considered scenario.

In the following section, we briefly elaborate the intensity based registration process along with the registration metrics under consideration. Further, we perform all the necessary analysis to meet the above enlisted objectives followed by discussion and conclusions made from the accomplished work.

2. INTENSITY BASED REGISTRATION

Intensity based registration between two images is achieved by maximizing a similarity metric (S) between the two images (equation 1). Similarity metric S considered here are mutual information and cluster reward algorithm.

2.1 Mutual Information

Mutual information has evolved from the field of information theory. MI describes a statistical dependence between two random variables (e.g. A and B) expressed in terms of variable entropies. Normally, Shannon entropy (additive in nature) is utilized to represent variable entropies (information content) and for this case mutual information between two variable A and B is defined as (Wachowiak, 2003)

$$MI\left(A,B\right)=H\left(A\right)+H\left(B\right)-H\left(A,B\right) \tag{2}$$

Above, H(A) and H(B) are the Shannon entropies of A and B respectively, H(A, B) is the joint entropy of B and A. Considering two remote sensing images to be registered as the two random variables, MI is a symmetric relation that always achieves values greater than zero. Registration of two images A and B is based on maximization of MI (A, B) (Equation 2). The marginal entropies and the joint entropy can be computed from the estimated joint histogram according to formulations described in (Chen et al., 2003a). For the presented work we have employed the normalized MI implementation proposed by Studholme et al. (1999). The utilized metric reduces the sensitivity of MI towards changes in image overlap.

$$MI(A,B)=\left(H(A)+H(B)\right)\big/H(A,B) \tag{3}$$

2.2 Cluster Reward Algorithm

Cluster reward algorithm is again dependent on the concept of joint histogram estimation between the images being registered. This metric utilizes both the joint histogram and individual histogram of the two images. The similarity measure IB_{craB} is defined as,

$$I_{CRA}=\left[\frac{\frac{\Phi}{F}-\frac{F}{P^2}}{1-\frac{F}{P^2}}\right] \tag{4}$$

Where,

$$\Phi=\sum_{k=0}^{N-1}\sum_{l=0}^{N-1}H_{RI}^{2}\left(k,l\right) \tag{5}$$

$$F = \sqrt{h_R h_I} \tag{6}$$

$$h_R = \sum_{k=0}^{N-1} H_R^2(k) \tag{7}$$

$$h_I = \sum_{k=0}^{N-1} H_I^2(k) \tag{8}$$

$$P = \sum_{k=0}^{N-1}\sum_{l=0}^{N-1} H_{RI}(k,l) \tag{9}$$

Where HB_{RIB} is the joint histogram of the reference and the input images, HB_{RB} and HB_{IB} are the histograms of the reference and the input images and N is the size of the images being registered. The parameter IB_{CRAB} needs to be maximized for achieving registration between images A and B.

For optimizing the similarity metric function, input image might be transformed several times over the reference image grid. However, in many cases, the transformed input image might not coincide with the target reference image grid. Therefore, an exact joint histogram may not be obtained and some approximation becomes inevitable. For the presented work one step joint histogramming technique namely generalized partial volume estimation (GPVE) (Chen and Varshney, 2003; Suri and Reinartz, 2008) has been utilized. Once a suitable technique for robust joint histogram estimation has been selected the critical task of finding the registration parameters accurately is left to an optimizer (Hua et al., 2003; Chalermwat et al., 1999; Cole Rhodes et al., 2003a, 2003b).

3. EVALUATION FOR HIGH RESOLUTION IMAGERY

For analysis purposes, two main challenges of enormous data volume and increased gap in different sensor geometries have been first dealt separately and then combined to form a practical registration scenario (section 4) to strengthen the understanding in functioning of the analyzed metrics.

3.1 Data Volume

Fortunately, the intensity based metrics when combined with simple compression techniques can achieve meaningful registration results in quick time and this has been demonstrated in this section of the paper. We present here the metric performances for an image pair extracted from TerraSAR-X and IKONOS-2 scenes acquired over west of Munich, Germany. The details of the selected dataset are tabulated in Table 1 (orthorectified scenes but georeferencing differences exist). Both the images compressed to different resolution levels using the mean block filter can be visualized in Figure 1.

	TerraSAR-X	**IKONOS-2***
Mode	High resolution spot light (HS)	Reverse Scanning
Spectral Resolution	9.65 GHz	450 – 900 nm
Pixel Spacing	1m	1m (panchromatic)
Bits per pixel	16 bit	11 bit
Date of Acquisition	25/12/07	14/10/07
Processing Level	Enhanced ellipsoid corrected using a DEM	Standard geometrically corrected

*Dataset courtesy of European Space Imaging

Table 1: Details of TerraSAR-X and IKONOS-2 Imagery (Dataset 1 and 2).

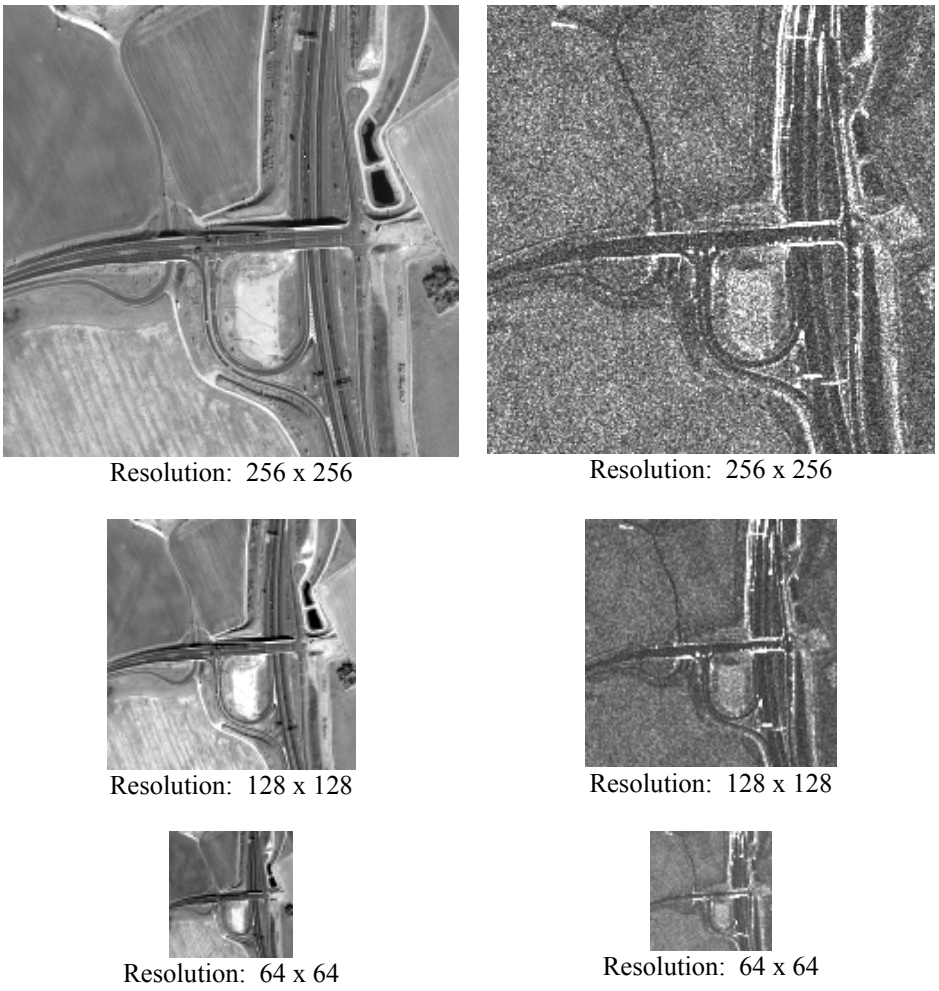

Figure 1: IKONOS-2 and TerraSAR-X imagery compressed to different resolution levels. (Original resolution of 512x512 pixels not displayed).

We present the results for original 1m (pixel spacing) images as well images compressed to coarser resolutions using averaging block filter. For experimentation purposes, we fix our reference image (TerraSAR-X) and move our input image (IKONOS-2) over the reference grid from [-20 20] pixels both in x and y direction at different resolution levels. At every image movement (sub-pixel) the similarity metric value (MI and CRA) has been plotted and the parameters producing the peak of the surface generated are assumed to be the correct registration parameters (theoretical assumption). For analysis, the joint histogram of various bin sizes has been estimated using the GPVE technique (Quintic B-spline kernel has been utilized for this analysis as more commonly utilized Cubic B-spline kernel yielded interpolation artifacts (Tsao, 2003; Inglada et al., 2007)).

Resolution	Bin Size	MI	CRA	No. of Evaluations	TAT
64 x 64	32	(14.00, -6.00)	(14.00, 2.00)	-	-
	64	(12.00, 2.00)	(12.00, 2.00)	-	-
	128	(12.00, -2.00)	(14.00, -2.00)	25921	13 mins
128x128	32	(12.00, -5.00)	(12.00, -5.00)	-	-
	64	(12.00, -5.00)	(12.00, -4.00)	-	-
	128	(12.00, -3.00)	(12.00, -2.00)	25921	55 mins
256x256	32	(12.0, -5.5)	(12.0, -6.0)	-	-
	64	(12.0, -6.0)	(14.0, -6.0)	-	-
	128	(12.50, -5.0)	(14.50, -4.0)	25921	4 hrs
512x512	32	(12.0, -6.0)	(15.0, -5.0)	-	-
	64	(11.5, -5.5)	(9.0, -4.0)	-	-
	128	(11.5, -5.5)	(11.5, -3.0)	6561	4 Hrs

Table 2: Registration peaks along with their computation time obtained for TerraSAR-X and IKONOS image pairs at different resolution levels.

Joint histogram bin size does not make a significant difference in TAT at same resolution levels; all the experiments have been done on Genuine Intel Pentium D CPU (2.8 GHz) with 2 GB RAM

The results for various resolution images tested in the above explained scenario can be visualized in Table 2. A typical behavior of intensity based techniques can be observed by alongside tabulated registration turn around times (TAT) which shows a drastic increase with an increase in mage resolution. A strong observation to be made is about the fact that fairly accurate registration parameters can be obtained from coarser resolution images in far less execution time. The normalized search spaces generated by the two metrics for bin size 128 can be visualized in Figure 2. Careful observations of the search spaces generated by the two metrics indicate the presence of local maxima in the search spaces and this problem is more profound for CRA as compared to MI. It is also observed that CRA function is more susceptible of pixel a displacement which is inferred from a larger range of CRA values (z axis) as compared to the values obtained by MI.

3.2 Different Sensor Geometries

To demonstrate the influence of different sensor geometries on intensity based registration we perform our analysis with high resolution imagery acquired over sub urban area in west of Munich, Germany. The images can be visualized in Figure 3 (a, b), the imaged scene has urban settlement situated very next to vast agricultural fields providing an opportunity to analyze the similarity metric performance for the land covers both combined and independent. For experimentation the following two scenarios have been considered:

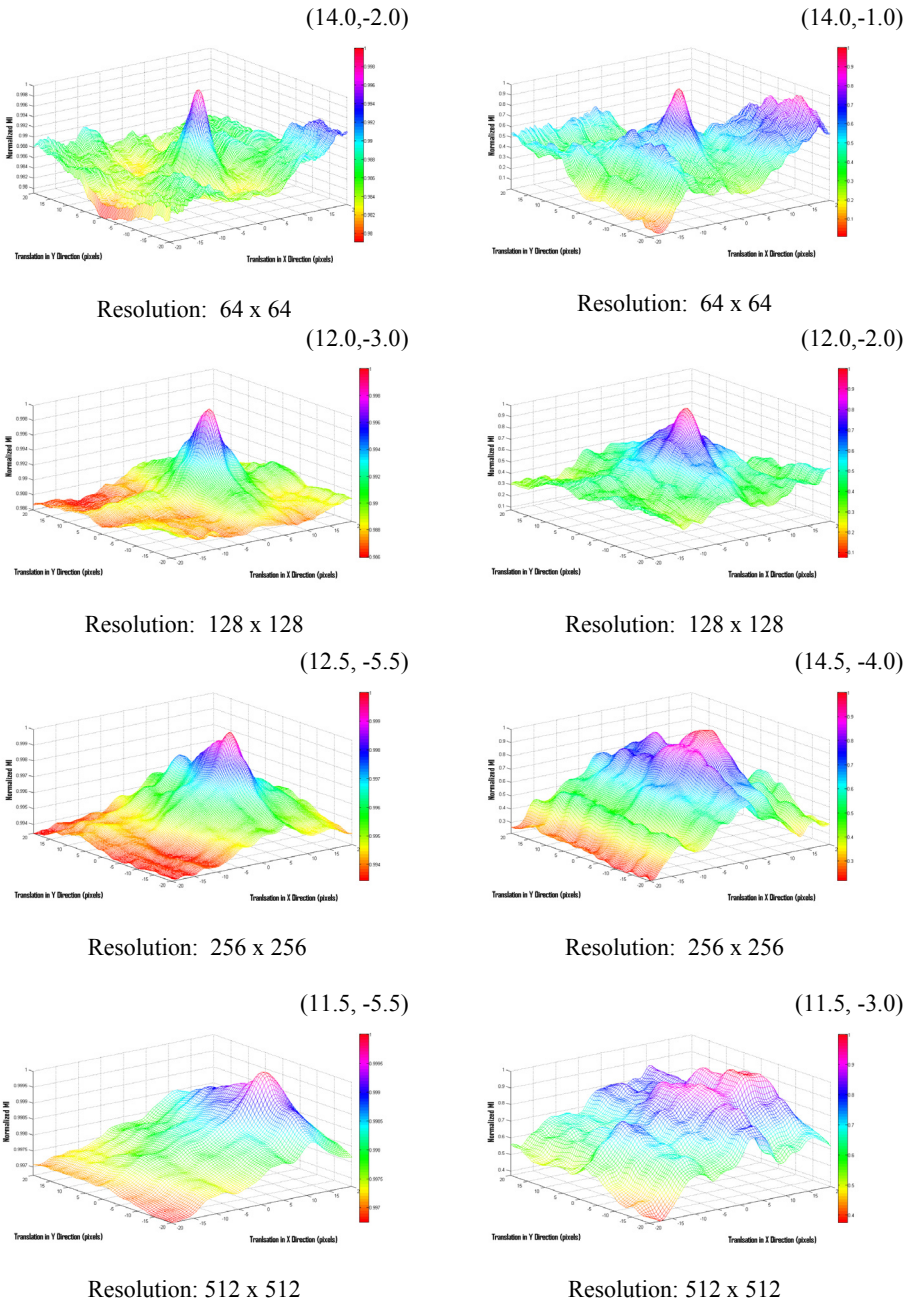

Figure 2: MI (left) and CRA (right) search spaces generated for different resolution image pairs. It is observed that fairly accurate registration errors (top right) present within the image pairs could be estimated from compressed coarser resolution images.

1) For case 1, we select pixels only from the plain fields (roughly demarcated with rectangle in Figure 2) in both the images for computing the registration parameters (Size: 953x1096 pixels). For the plain field pixels the side ways looking SAR sensor and the downward looking optical sensor are not expected to have much of their geometric influence, so favorable registration results as in the previous case are expected.
2) For case 2, we select the entire image scene for registration parameter computation and hence analyze the influence of the sub urban establishments on similarity metric performance (Size: 1001 x 2001 pixels). The urban establishments cause great changes in SAR image radiometry due to its sideways looking geometry.

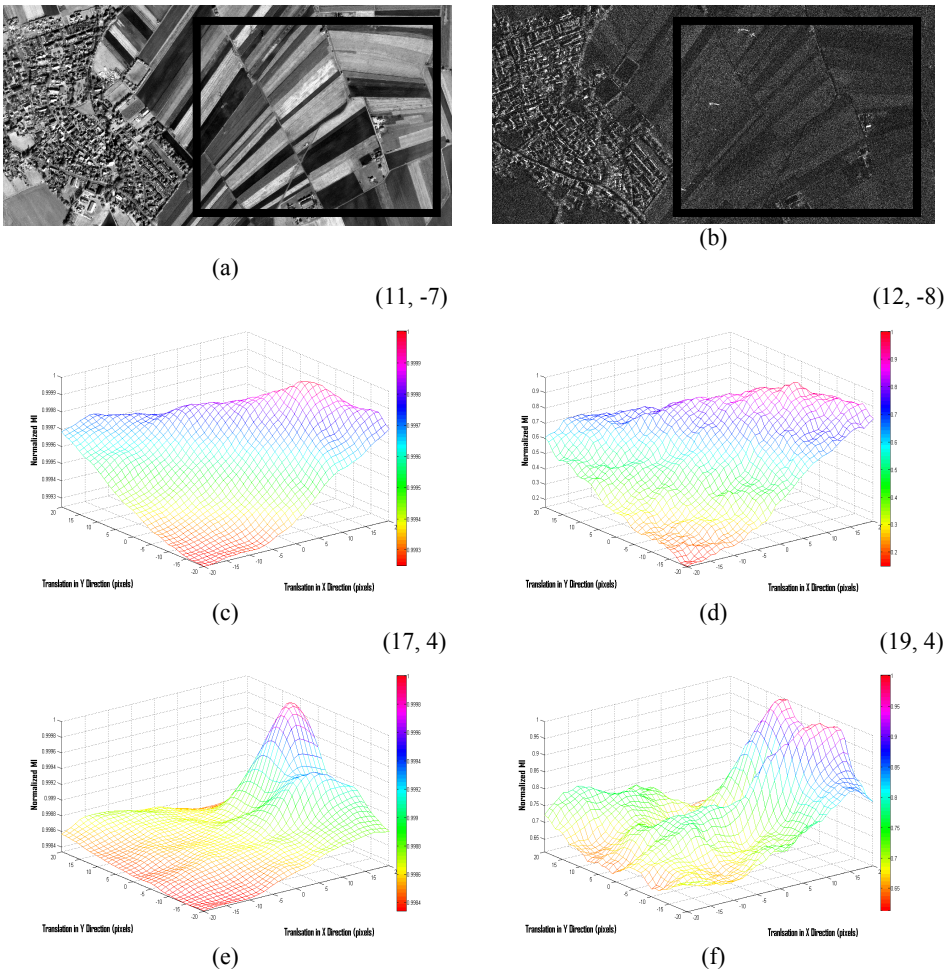

Figure 3: The IKONOS (a) and TerraSAR-X (b) imagery for dataset 2. Plain field pixels lead to a registration peak of (11, -7) for MI (c) and (12, -8) for CRA.(d). Introduction of urban area pixels shifted the registration peaks for MI and CRA to (17, 4) (e) and (19, 4) (f) respectively.

Here also we move the input image (IKONOS-2) again over the reference image grid (TerraSAR-X) in the range [-20 20] pixels in both x and y direction, both the similarity metric functions have been recorded at integral pixel movements. For this experiment, joint histogram of bin

size 64 has been estimated using the GPVE technique (Cubic B-spline kernel). The search spaces generated by both the metrics for the two cases are provided in Figure 3. The Figure 3c and 3d represents the generated search spaces for MI and CRA while utilizing pixels belonging only to the land cover class fields. Figures 3e and 3f represent the generated search spaces while utilizing the complete image region including the sub urban establishments

Tests conducted with a bin size 64 only taking pixels from the plain fields, returned the registration peak at (11, -7) and (12, -8) for MI and CRA respectively (Figure 3c, 3d). On the other hand, the surfaces generated by utilizing all the pixels in both the images obtain a peak at (17, 4) and (19, 4) for both MI and CRA respectively (Figure 3e, 3f). A visual analysis using an overlay tool clearly indicates the present misalignment within the imagery after using the obtained registration parameters from case 2. Although the land cover fields constitute more than 53% of the total image area but still the introduction of the urban area pixels have derailed the registration process which is evident in the form of false registration peaks observed. This shift in the peaks can be attributed to high entropy content normally present with in urban areas which is also evident from the sharper false registration peaks obtained by both the similarity metrics in case 2. As was the observation made in the previous dataset, local minima and surface roughness is more profound in the CRA search spaces generated for two different cases in dataset 2.

This shift in the registration peaks of both the metrics can directly be related to the introduction of region greatly influenced by different sensor geometries. Theoretically, registration between two images is achieved by maximizing the similarity metric between two images. But due to the influence of different sensor geometries especially in urban, semi urban areas the peak obtained simply by the maximization process might not yield desirable results. The double bounce, triple bounce effect prominently observed in the SAR imagery at 1m resolution make the radiometric information produced by two sensors incompatible in urban areas and might lead to failure of intensity based techniques to detect correct registration parameters.

Normally, for practical applications land cover classes are hardly as segregated as available in the analyzed dataset. However, the presented scene is still a good selection to show the possible influence of different sensor geometries on an intensity based registration performance. This problem of mixed classes asks for a segmentation step before using intensity based techniques for registration parameter estimation. The segmentation should be targeted to incorporate only those pixels in the registration process which are not influenced by different sensor geometries (like the plain field pixels in dataset 1 and 2). However, the idea of introducing a segmentation step before performing an intensity based registration has the following concerns to be addressed:

i. Supervised or unsupervised, ideally unsupervised would be preferred to avoid any kind of manual intervention in the registration process
ii. The accuracy and the speed of the segmentation, it needs to be established that how much accuracy in segmentation is actually needed for robust performances.
iii. Segmentation required only in one image or both the images involved in the registration process

Considering the scenario, we propose here a method to successfully adapt intensity based techniques for heterogeneous land cover scenes. The proposed method is unsupervised, very fast and easy to implement and requires segmentation in only one of the images being registered. The idea of the proposed solution lies in the histogram of a SAR image acquired over urban/semi-urban areas. Normally, the pixels produced by the double/triple bounce phenomenon result into a very strong backscatter to the radar sensor and thus these pixels always would be situated near the higher end of a SAR image histogram. Here this has to be kept in mind that certain other pixels (not generated by the SAR geometry), due to constructive interference of the radar waves can also produce high intensity

value (strong backscatter). However, it still might be possible to bin out most of the pixels explicitly generated due to the SAR sensor geometry using histogram thresholds. As already mentioned certain pixels (even in plain fields) as a result of constructive interference might also be binned out of the registration process. But as long as the numbers of such false pixels being binned out represent minority of the total pixel population, the registration peaks obtained by the similarity metrics are not expected to change. The number of such pixels can definitely be reduced by some kind of speckle filtering but intensity based registration of SAR and optical imagery does not require any necessary smoothing step so we refrain to perform the same in the presented approach.

To perform the necessary segmentation step we again revert to image compression, the advantages of performing the segmentation task in a coarser resolution SAR image are two folds:

i. Computational speedup: It is clear that the time complexity of the segmentation step is directly dependent upon the size of the image so image compression can be used to a good effect.
ii. Image Smoothing: The utilized averaging block filter also introduces some kind of smoothing in the image so this in turn might help only binning out those pixels which are a result of sideways looking SAR sensor geometry

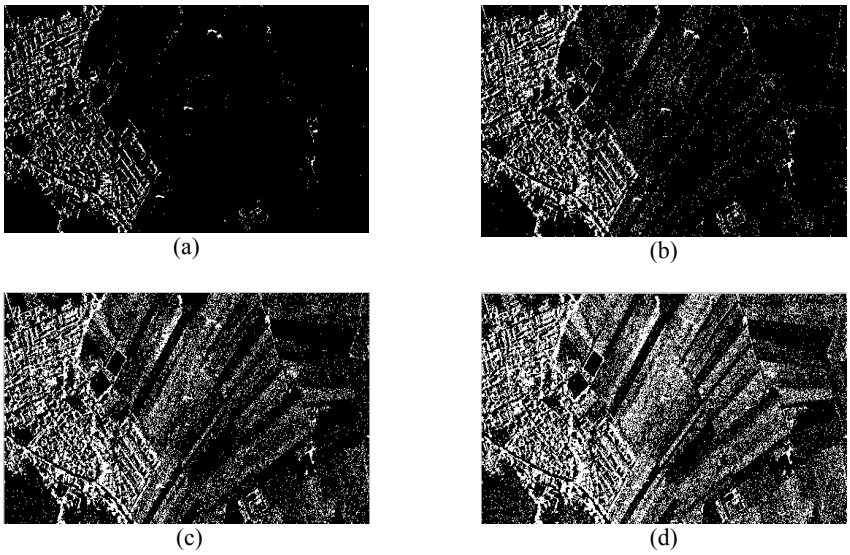

Figure 4: Pixels with value 1 were left out (in SAR image) of the registration process after introducing high thresholds of 5% (a) 10% (b) 20% (c) and 30% (d) at image compressed to one-forth of its original resolution (Dataset 2).

The proposed segmentation performed here can be visualized in Figure 4. First the SAR image (Figure 2b) is down-sampled to one-forth of its original resolution. The histogram of the obtained down-sampled image is now used to generate thresholds for binning out possible pixels generated by the SAR sensor geometry in the original resolution image. To realize the goal of the segmentation process thresholds are made from the higher end of the image histogram.

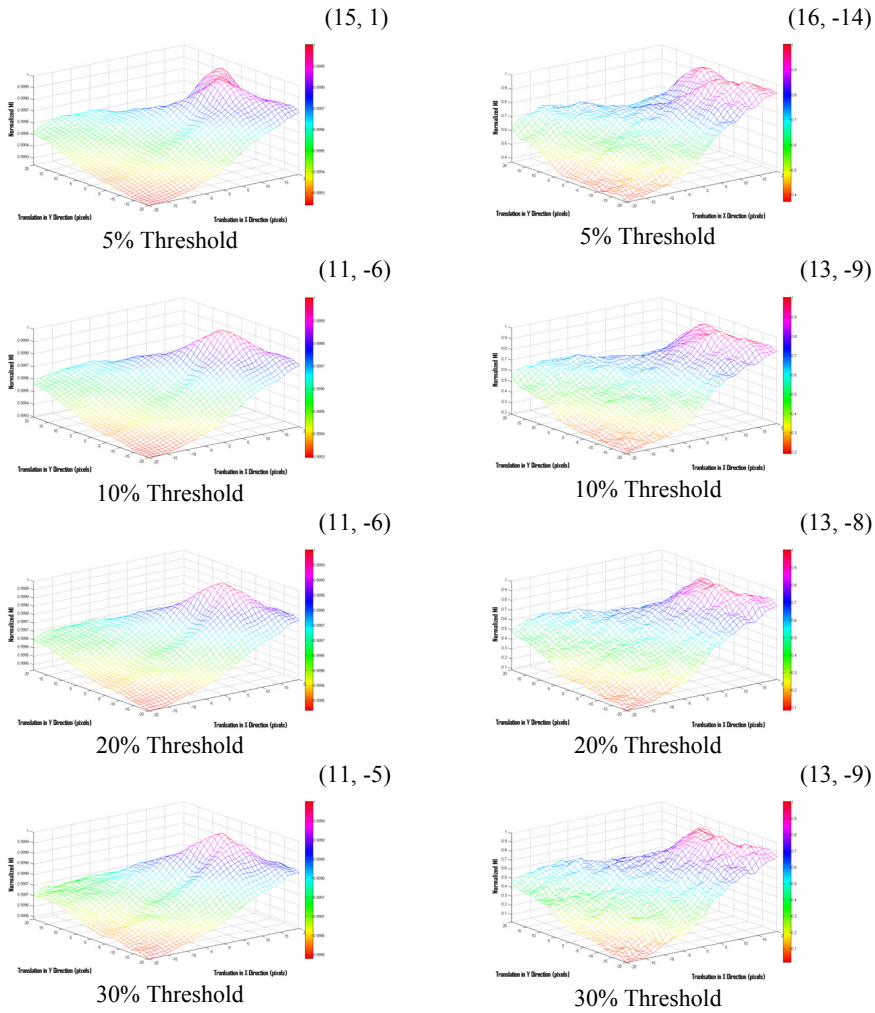

Figure 5: Registration surfaces generated by MI (left) and CRA (right) between segmented SAR (using masks in Figure 4) and the original optical image.

The result of this segmentation scheme has been represented as binary masks (value of 1 means the pixel is not included in the registration process) depicted in Figure 4 (a, b, c, d) represent the results of introducing thresholds of 5, 10, 20 and 30% on the down-sampled image (one-fourth of the original resolution). It can be clearly observed that as the threshold limit is relaxed more and more pixels from the plain fields start coming into the undesired pixel category and this might have an adverse influence on similarity metric performance.

To analyze the influence of the performed segmentation we repeat the same experiment as done earlier. The idea here is to register the segmented SAR image with the corresponding optical image. In this scenario all the pixels from optical imagery would contribute to the similarity metric statistics but from the SAR imagery only those pixels which are within the threshold limits (assigned the value 0 in the masks of Figure 4) would participate in the registration process. To analyze the threshold value influence on the final registration results and similarity metric performances we repeat the same

experiment with different threshold levels (Figure 4). The similarity metric surfaces generated in the search space of [-20 20] pixels for the segmented SAR images and the original optical image have been provided in Figure 5 for visualization and analysis

The influence of the introduced segmentation step prior to intensity based registration is evident on the registration search spaces generated by the two metrics in Figure 5. Segmentation of the SAR image using the mask depicted in Figure 4a (5% threshold) influenced the registration peaks observed in Figure 3e and 3f significantly. The registration peaks obtained by MI and CRA (17, 4) and (19, 4) in Figure 3e and Figure 3f were shifted to (15, 1) and (16, -14) respectively. Further segmentation of the SAR image i.e. using threshold in the order of 10, 20 and 30% percent yielded almost the same registration peaks as were reported by the similarity metrics using only the pixels from plain fields (Figure 3c and Figure 3d). The MI and CRA peaks obtained for the segmented SAR and the optical imagery deviate only about 1m from the peaks obtained earlier using only the plain field pixels, which in this case are assumed to be the true on ground registration parameters.

The segmentation strategy introduced in this section has yielded encouraging registration performances from both the similarity metrics. It can be observed that very loose threshold of 5% could remove only some of the pixels influenced by the SAR senor geometry and thus did not produce expected registration results. On further tightening the thresholds to higher levels most of the pixels influenced by SAR sensor geometry (mostly in the urban settlement) were removed and expected registration parameters were successfully retrieved.

4. REGISTRATION IN URBAN AREAS

In this section, we present our analysis using a scenario which the decision makers and end users might have to confront with while utilizing high resolution images acquired over urban areas. We consider TerraSAR-X and IKONOS imagery acquired over the city of Sichuan in China (post earthquake) (dataset details in Table 3). The image pairs have been procured from georeferenced and orthorectified scenes (without DEM) and have a georeferencing error of approximately 90m in x direction and 45m in y direction (rough estimates).

	TerraSAR-X	**IKONOS-2**
Mode	High resolution spot light	Reverse Scanning
Pixel Spacing	1m	1m (panchromatic)
Bits per pixel	16 bit	11 bit
Image Size	923 x 942	923 x 942
Angle	Incidence Angle 50.80°	Nominal Collection Elevation: 59.26°
Date of Acquisition	15/05/08	28/06/8
Processing Level	Geometrically corrected using an ellipsoid	Standard geometrically corrected

Table 3: Details of the TerraSAR-X and IKONOS-2 Imagery acquired over China

The images in compressed and enhanced form have been provided for visualization in Figure 6a and 6b. A small road intersection from the two images overlaid using a GIS overlay tool to visualize the georeferencing error has been provided in Figure 6c. The complexity of manually correcting the present registration errors can be visualized in Figure 6d and 6e where the city road intersection in the middle of the analyzed scene has been provided. Due to fine minute details now available with the high resolution sensors, the idea of finding the same control/tie point (road intersections) in the small area displayed becomes much more challenging than ever before.

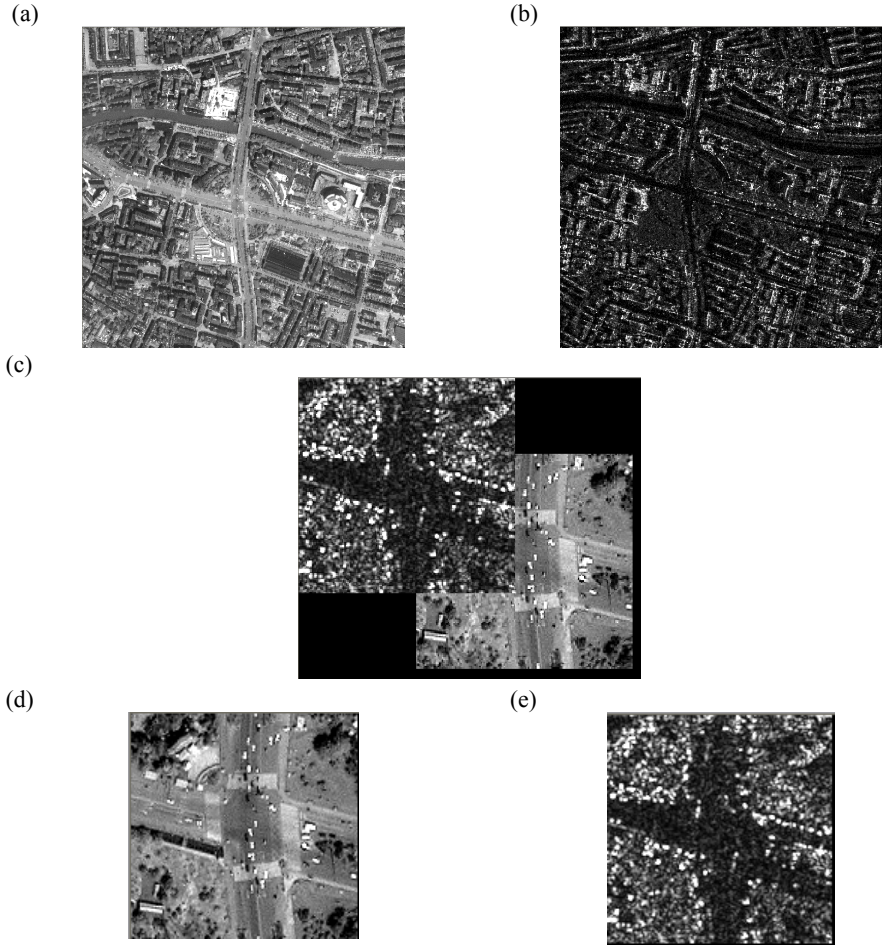

Figure 6: (a) Compressed and enhanced IKONOS image. (b) Compressed and enhanced TerraSAR-X image. (c) Existing georeferencing differences depicted by overlaid road intersections from the two images using a GIS overlay tool. (d) Sample road intersection from IKONOS image. (e) Same road intersection from TerraSAR-X image.

To continue with the analysis we perform the same registration experiments as performed for the two previous datasets. According to the rough registration differences observed, we translate the input IKONOS image over the reference TerraSAR-X image in a range of -120 to -80 pixels (meters) in x and -65 to -25 pixels (meters) in y direction. The true registration parameters are expected to lie within this range but without the knowledge of any ground truth these cannot be estimated. For a consistency and behavioral analysis, all the computations have been made from a 128 bin size joint histogram estimated through cubic B-spline kernel.

To analyze the influence of the SAR images pixels generated mainly by double bounce effect in urban areas we performed the same segmentation scheme introduced for the previous dataset. We have segmented the SAR image using thresholds in range 5 to 60% (Figure 7) to obtain the registration peaks tabulated in Table 4. It can be visualized in various masks that most of pixels

influenced by the sideways looking SAR sensor geometry are binned out for different threshold levels (Figure 7).

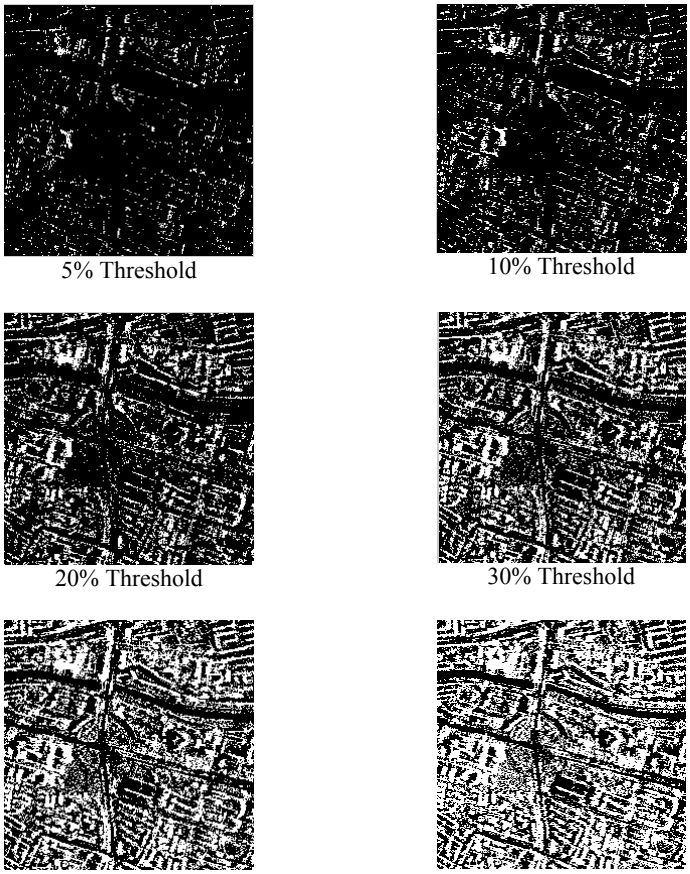

Figure 7: Pixels with value 1 were left out (in SAR image) of the registration process after introducing high thresholds of 5 to 50% at image compressed to one-forth of its original resolution (Dataset 3).

	MI	**CRA**
Original image pairs	(-80, -46)	(-99, -61)
SAR 5% TH*	(-80, -46)	(-95, -60)
SAR 10% TH	(-96, -47)	(-96, -60)
SAR 20% TH	(-96, -47)	(-95, -59)
SAR 30% TH	(-96, -47)	(-96, -44)
SAR 40% TH	(-96, -47)	(-112, -59)
SAR 50% TH	(-103, -49)	(-112, -59)
SAR 60% TH	(-99, -48)	(-112, -59)

*Threshold

Table 4: Registration peaks achieved by both the similarity metrics for the original image pairs and segmented SAR and optical image.

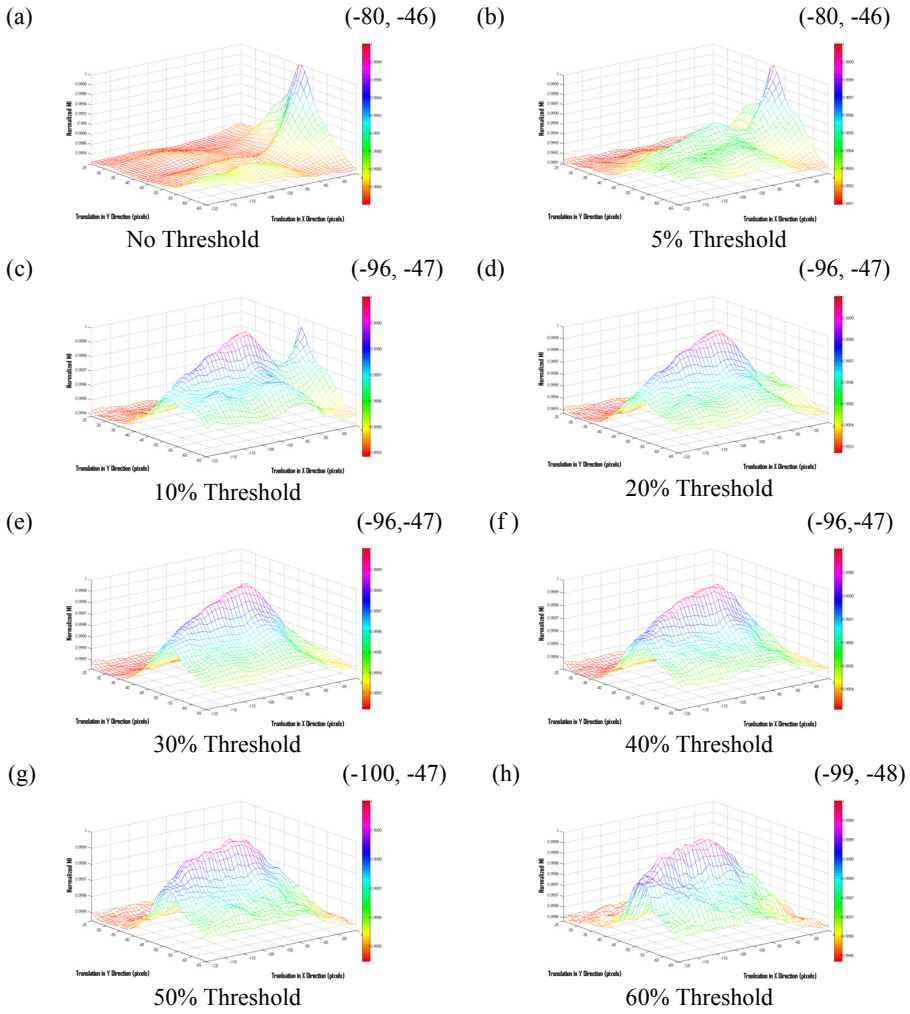

Figure 8: Registration surfaces generated by MI between original SAR-optical image (Figure 6a and 6b) pairs and segmented SAR images (masks in Figure 7) and the original optical image for dataset 3.

We first test the metric performance for the original images and then for segmented SAR image and the optical image. As observed for the previous dataset in this case also the registration peak obtained for the original imagery shifts as the pixels influenced from the SAR geometry are removed from similarity metric computation.

Results in Table 4 indicate a consistent MI performance as after recording a peak at (-80, -47) for original images the registration peak at (-96, -47) is consistent from 10 to 40% threshold introduced in the SAR imagery. As observed for previous datasets the MI search surfaces generated here were also found to be much smoother than the corresponding CRA surfaces. For detailed analysis and brevity only the MI surfaces generated between segmented SAR and the optical image are being provided in Figure 8.

A careful observation of the generated MI search spaces in Figure 8 clearly indicates a systematic shift of registration peak from (-80, -47) to (-96 -47) pixels in x and y direction. For the original images and 5% high thresholded SAR image the peak is at (-80, -47) pixels. A small local maxima is observed around (-96, -47) is observed for 5% threshold image which becomes more profound for 10% thresholded SAR image. Further thresholding of the SAR image (till 40%) makes the registration peak stable at (-96, -47) pixels in x and y direction. As further information in form of pixels taking part in the registration process from the SAR image are removed (threshold 50 and 60%) the MI registration search space is observed to be rough and the peak also show small shifts in both x and y directions.

Further, we also explore the important capability of the analyzed intensity based metrics (estimation of rough registration parameters through compressed images, highlighted from the analysis of dataset-1). The images depicted in Figure 6a, b were compressed to one forth of their original resolution and registration parameters have been exhaustively searched between the original SAR and optical image and as well as the different segmented SAR and optical image. The detailed findings have been tabulated in Table 5. It is observed that the important property of the similarity metrics to estimate rough registration parameters from compressed images is also observed here for the original images pairs and various thresholded SAR images (20, 30 and 40%) and the original optical image. An important observation about the CRA metric is that it achieves similar registration peaks as MI for compressed images but it performance deteriorates higher up the image pyramid. This trend was observed even for dataset-1 where CRA showed certain anomalies for the highest resolution imagery and for this dataset also for resolution level L2 the registration peaks obtained by various image pairs are almost similar to MI but as the resolution is improved the CRA registration peaks show a drift and an inconsistent overall behavior.

		L2	**L1**	**L0**
Image Size		250 x 250	500 x 500	999 x 999
Pixel Spacing		4m	2m	1m
Search Space (pixels)		x: -30 to -20 Y: -17 to -7	X: -60 to -40 y: -33 to -13	x: -120 to -80 y: -65 to -25
Original Image Pairs	MI	(-20.00, -11.50)	(-40.0, -23.0)	(-80, -47)
	CRA	(-24.50, -14.75)	(-49.0, -30.0)	(-99, -61)
20% High Threshold	MI	(-24.00, -12.00)	(-49.0, -24.0)	(-96, -47)
	CRA	(-24.00, -11.75)	(-48.0, -22.5)	(-95, -59)
30% High Threshold	MI	(-24.00, -12.00)	(-49.0, -24.0)	(-96, -47)
	CRA	(-24.00, -12.00)	(-48.0, -22.5)	(-96, -44)
40% High Threshold	MI	(-24.00, -12.00)	(-50.0, -24.0)	(-96, -47)
	CRA	(-24.00, -12.00)	(-55.0, -29.0)	(-112, -59)

Maximum registration accuracy at all registration levels is 1m

Table 5: Registration peaks reported by the similarity metrics at various resolutions between original SAR-optical and segmented SAR-optical image pairs (Dataset 3).

The second dataset from Germany highlighted the metric behavior where after introducing the explained segmentation step correct assumed on ground registration parameters could be retrieved for various threshold levels. The similar metric behavior was also reported for these urban area images acquired over the city of Sichuan in China. Here we assume the registration parameters reported by MI (-96, -47) for threshold levels of (10 to 40%) as possibly the correct registration parameters. We transform our input IKONOS image over the reference image grid according to the obtained parameters and the images have been check squared in Figure 9 for visualization. It is clear from the discussed process that most of the pixels participating in the registration scheme are intended to be from the on ground features (roads, river etc) and thus they are expected to show good registration in both the images.

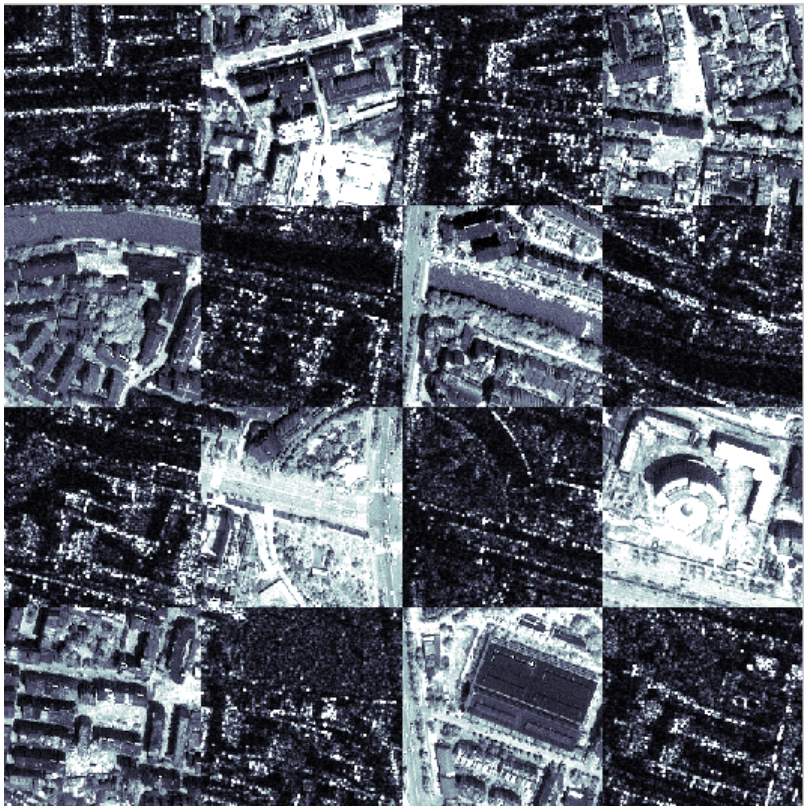

Figure 9: Registered TerraSAR-X and IKONOS imagery from dataset-3. The IKONOS image has been transformed by -96 pixels in x direction and -47 pixels in y direction. The common area of size 800x800 pixels is displayed at 50% of the original size.

5. DISCUSSION AND CONCLUSIONS

For combined utilization of data from diverse natured sensors automatic co-registration methods are a must as satellite images may have georeferencing differences of magnitude that might influence any analysis or decision making process. Considering the meticulous task of extracting and matching conjugate features in SAR and optical imagery (especially metric resolution imagery) a general feature based image registration technique for various scenarios might be difficult to develop and implement. On the other hand, the intensity based metrics for medium resolution images (5-15m GSD) have shown enough potential of suitably being modified and extended for different registration scenarios.

In this paper we have investigated the performance of intensity based registration techniques for metric resolution imagery acquired by TerraSAR-X and IKONOS-2 satellites. As was expected the different radiometric information contained in the two images due to enormous amount of fine details did hamper the intensity based techniques but suitable solutions have been proposed for handling the same. Due to unavailability of true registration parameters, we have not been able to perform accuracy analysis for our registration results. In accordance to the laid down objectives in section 1, the needful analysis has been made to report the following conclusions

i. Intensity based techniques have shown capabilities to estimate quite accurate registration parameters even from down sampled image pairs. The presented analysis only considered two translations as the registration parameters but this property is also observed even when a rotational difference also exists with in the datasets (Suri et al., 2009).

ii. The influence of difference sensors geometries is more profound for urban settlements as compared to the plain areas. The intensity based metrics have shown enough capabilities of handling this difference through segmentation steps introduced only in SAR image. As the registration peaks were observed to be consistent for different threshold levels for two datasets it can be safely inferred that accuracy of segmentation is not a very strict criteria for similarity metric performances. In general, we can also introduce urban area detection in one of the images and expect to retrieve accurate registration parameters using the depicted analysis.

iii. A comparative evaluation between the two considered metrics depicts mutual information as a more robust metric for different registration applications. Cluster reward algorithm search spaces generated for three datasets were found to be inconsistent in some cases and suffered from artifacts and local maxima.

BIBLIOGRAPHY

Brown, L.G., (1992). A survey of image registration techniques, ACM Computing Surveys, 24, 4, pp.325-376

Chalermwat, P., El-Ghazawi, T., and LeMoigne, J., (1999). GA-based parallel image registration on parallel clusters In: Proceedings *IPPS/SPDP Workshops* pp. 257-265

Chen, H., and Varshney, P.K., (2003) Mutual information-based CT-MR brain image registration using generalized partial volume joint histogram estimation. IEEE Transactions on Medical Imaging, 22, pp. 1111-1119

Chen, H., Varshney, P.K., and Arora, M.K., (2003a) Mutual information based image registration for remote sensing data. International Journal of Remote Sensing, 24, 18, pp. 3701-3706.

Chen, H., Varshney, P.K., and Arora, M.K., (2003b) Performance of mutual information similarity measure for registration of multitemporal remote sensing images. IEEE Transactions on Geoscience and Remote Sensing, 41, 11, pp. 2445-2454.

Cole Rhodes, A.A., Johnson, K.L., LeMoigne, J., and Zavorin, I., (2003a) Multiresolution registration of remote sensing imagery by optimization of mutual information using a stochastic gradient. IEEE Transactions on Image Processing, 12, 12, pp. 1495-1511

Cole Rhodes, A.A., Johnson, K.L., and LeMoigne, J., (2003b) Image registration using a $2P^{nd}$ order stochastic optimization of mutual information. In: Proceedings Geoscience and Remote Sensing Symposium, Toulouse, France, pp. 4038-4040

Fonseca, L. M. G., and Manjunath, B. S., (1996) Registration techniques for multisensor remotely sensed imagery. Photogrammetric Engineering and Remote Sensing, 62, 9, pp. 1049-1056

Hua X., Pierce, L.E., and Ulaby, F.T., (2003) Mutual information based registration of SAR images. In Proceedings of the IGARSS'03, 6, pp.4028- 4031, 28 June - 02 July, Toulouse, France

Inglada, J., (2002) Similarity measures for multisensor remote sensing images, In: Papers presented at the IGARSS 02, June 24 – 28, Toronto, Canada, CD ROM Proceedings.

Inglada, J., and Giros, A., (2004) On the possibility of automatic multisensor image registration. IEEE Transactions on Geoscience and Remote Sensing, 42, 10, pp. 2104-2120

Inglada, J., Muron, V., Pichard, D., and Feuvrier, T., (2007) Analysis of artifacts in subpixel remote sensing image registration. IEEE transactions on Geoscience and Remote Sensing, 45, 1, pp. 254-264

Li, W. Li, X., Wu, Y., and Hu, Z., (2006) A novel framework for urban change detection using VHR satellite images. Pattern Recognition, 2, pp. 312 – 315

Reinartz, P., Lachaise, M., Schmeer, E., Krauss, T., and Runge, H., (2006). Traffic monitoring with serial images from airborne cameras. ISPRS Journal of Photogrammetry and Remote Sensing 61, 3-4, pp.149-158

Simoncelli E.P., and Freeman W.T. (1995) The Steerable Pyramid: A Flexible Architecture for Multi-Scale Derivative Computation. In Proceedings: IEEE Second International Conference on Image Processing. Washington DC, October 1995

Stramondo, S., Bignami, C., Pierdicca, N., and Chini, M., (2007) SAR and optical remote sensing for urban damage detection and mapping: case studies. In: Proceedings of Urban Remote Sensing Joint Event, Paris, France, pp.1-6

Studholme, C., Hill, D.L.G., Hawkes, D.J., (1999) An overlap invariant entropy measure of 3D medical image alignment. Pattern Recognition, 32, 1, pp. 71–86

Suri, S., and Reinartz, P., (2008). Application of generalized partial estimation for mutual information based registration of high resolution SAR and optical imagery. In: paper presented at the 11th International Conference on Information Fusion, June 30- July 3, Cologne Germany, CD-Rom Proceedings

Suri, S., Schwind, P., Reinartz, P., and Uhl, P., (2009). Combining mutual information and scale invariant feature transform for fast and robust multisensor SAR image registration. In: papers presented at the 75th ASPRS annual conference, March 8 – 13, Baltmiore MD, USA, CD-Rom Proceedings

Tsao, J., (2003) Interpolation artifacts in multimodality image registration based on maximization of mutual information. IEEE Transactions on Medical Imaging, 22, 7, pp. 854-864

Wachowiak, M.P., Smolikova, R., and Peters, T.M., (2003). Multiresolution Biomedical Image Registration Using Generalized Information Measures, Lecture Notes in Computer Science 2879 (MICCAI 2003) pp. 846-853

Wong, A. and Clausi, D.A. (2007) ARRSI: Automatic registration of remote sensing images. IEEE Transactions on Geoscience and Remote Sensing, Vol. 45, No. 5, Part II, pp. 1483-1493

Zitová, B., and Flusser, J., (2003) Image registration methods: a survey. Image and Vision Computing, 21, 11, pp. 977-1000